Bull. Mater. Sci., Vol. 37, No. 3, May 2014, pp. 481–489. © Indian Academy of Sciences.

Characterization, dielectric and electrical behaviour of $BaTiO_3$ nanoparticles prepared via titanium(IV) triethanolaminato isopropoxide and hydrated barium hydroxide

RAVINDRA H UPADHYAY, ANANT P ARGEKAR† and RAJENDRA R DESHMUKH*

Physics Department, Institute of Chemical Technology, Matunga, Mumbai 400 019, India
†Department of Chemistry, Institute of Science, Fort, Mumbai 400 032, India

MS received 29 November 2012; revised 8 April 2013

Abstract. **A new sol-precipitation technique for the preparation of nano $BaTiO_3$ crystallite has been developed by reacting 0·2 M each of Ti(IV) triethanolaminato isopropoxide and hydrated barium hydroxide in methanol such that the molar ratio of Ba : Ti is 1·02 at 80 °C under stirring (1200 rpm) for one hour in alkaline media using tetra methyl ammonium hydroxide (TMAH). It was calcined at 100 °C for 12 h. Structural and compositional properties were investigated by XRD, SEM, EDX, TEM, SAED and DLS techniques. FT–IR and TG–DTA were used to characterize its purity and the thermal stability. The $BaTiO_3$ particles prepared were found to be spherical, homogeneous and cubic in structure. The particle size was found to be 23–31 nm. The dielectric constant and dissipation factor after sintering at 400 °C were 5379 and 0·63, respectively at 100 Hz frequency. The a.c. conductivity ($\sigma_{a.c.}$) was found to be 2×10^{-5} S-cm^{-1} at room temperature (30 °C). It increased with increasing temperature up to 50 °C and decreased with further increase in temperature. The impedance was $3{\cdot}37 \times 10^5$ ohms at room temperature. It decreased with increasing frequency.**

Keywords. **$BaTiO_3$ nanoparticles; XRD; SEM; TEM; DLS; dielectric constant.**

1. Introduction

$BaTiO_3$, is a well known and widely investigated dielectric material. It is mainly used in capacitors due to its high dielectric constant. The dielectric properties of $BaTiO_3$ are controlled by purity and microstructure which are dependent on the methods of preparation (Subbarao *et al* 1981; Frey and Payne 1996; Zhao *et al* 2004). Recent advances in nanotechnology such as MLCC, MEMS and DRAM have resulted in miniaturization of devices (Setter and Waser 2000). These require nanosize $BaTiO_3$. The nanosize $BaTiO_3$ are used in different polymers to prepare polymer nanocomposites for specific use (Kobayashi *et al* 2009; Hanemann *et al* 2011; Upadhyay and Deshmukh 2013). Various chemical routes like coprecipitation, sol-gel, sol precipitation, hydrothermal, reverse miscellar, etc. are known to yield nanoparticle products (Segal 1997; Guangneng *et al* 2005). The sol-precipitation method gives fine particle size, simple compositional control and low processing temperature.

The structural and physical properties of the nanoparticles are strongly dependent on selection of starting material, rate of hydrolysis and condensation, and processing temperature. Alkoxides are used as one of the precursors in sol precipitation. Longer chain of the alkoxide depresses the rate of hydrolysis. Ti(IV) triethanolaminato isopropoxide is easily available in the market and has been used for the synthesis of cerium titanium oxide (Feng *et al* 2006). Mechanism of hydrolysis of $Ti_3[(OC_2H_4)_3N]_4$ formed by reaction of titanium isopropoxide with triethanolamine to obtain TiO_2 nanoparticles through $Ti(OH)_4$ has been reported (Shahini *et al* 2011). However, there is no report for the synthesis of $BaTiO_3$ with Ti(IV) triethanolaminato isopropoxide. Therefore, Ti(IV) triethanolaminato isopropoxide was selected as the precursor for the preparation of $BaTiO_3$ by sol precipitation in the present work. The $BaTiO_3$ nanoparticles thus obtained were characterized by XRD, SEM, TEM, EDX, SAED, DLS, FT–IR and TG/DTA techniques and dielectric as well as electrical properties were investigated in this paper.

2. Experimental

2.1 *Materials*

All the chemicals and solvents used were of A.R. grade. $Ba(OH)_2{\cdot}8H_2O$ and formic acid (S.D. Fine Chem. Ltd, Mumbai, India), Ti(IV) triethanolaminato isopropoxide (Aldrich, USA), tetra methyl ammonium hydroxide (TMAH) (SRL, Mumbai, India) and methanol (Merck, Mumbai, India) were purchased from the local dealer. Deionized water was used throughout the work.

*Author for correspondence (rr.deshmukh@ictmumbai.edu.in)

2.2 *Procedure for preparation of $BaTiO_3$*

Methanolic solution of 0·2 M Ti(IV) triethanolaminato isopropoxide and aqueous solution of 0·2 M $Ba(OH)_2 \cdot 8H_2O$ were taken in a reacting vessel such that the molar ratio of Ba/Ti was 1·02. The mixture was heated to 80 °C and TMAH was added and stirred at 80 °C for 1 h continuously at 1200 rpm. The precipitate obtained was filtered quickly through centrifugation at 4000 rpm. It was washed first with methanol, dilute formic acid and then with water and finally with acetone.

The $BaTiO_3$ cake obtained was crushed and calcined at 100 °C for 12 h in an electric furnace. The powder was stored in a brown bottle and kept in a vacuum desiccator for its characterization and further investigation.

2.3 *Instrumentation*

X-ray diffractometer (XRD) (Model: 'X'Pert 'PRO', PANalytical) was used at 40 kV, 30 mA and sampling step 0·02 and 30 s integration time, using CuKα radiation of $\lambda = 0{\cdot}1542$ nm, for crystal structure determination. Scherrer's equation and PowderX software were used to evaluate and calculate the crystallite size and lattice parameters. The field emission scanning electron microscope (FE–SEM) (Model: JSM-7600F, Jeol) was used for morphological studies. Energy dispersive X-ray spectroscope (EDX) (Oxford Instrument) was used to find chemical composition. Transmission electron microscope (TEM) (Model: CM200, Philips) was used with accelerating voltage 200 kV and resolution 0·23 nm for study of morphology and size of the particles. Dynamic light scattering (DLS) instrument (Model: U2489ZS, Nanotrac) was used to study the particle distribution. Fourier Transform Infra Red Spectroscope (FT–IR) (Model: Spectrum 100, Perkin-Elmer) was employed for purity studies. Thermogravimetric and differential thermal analysis (TG–DTA) instrument (Model: Pyris Diamond, Perkin-Elmer) was used for thermal stability studies. Precision Impedance Analyzer (Model: 6500B, Wayne Kerr) was employed for investigating dielectric and electrical properties with component fixtures (Model: 1011).

3. Results and discussion

3.1 *Synthesis of barium titanate nanoparticles*

When Ti(IV) triethanolaminato isopropoxide was reacted with hydrated $Ba(OH)_2$ in aqueous methanol at 80 °C, four molecules of water and two hydroxyl ions were attached through their oxygen atoms to titanium of Ti(IV) triethanolaminato isopropoxide in a nucleophilic process formulating titanium hexahydroxide $[Ti(OH)_6^{2-}]$ complex ion, releasing one molecule of propanol and one molecule of triethanolamine in solution. $Ti(OH)_6^{2-}$ complex ion was then neutralized immediately by Ba^{2+} cation of $Ba(OH)_2$ in highly alkaline solution to form $BaTiO_3$. These reactions are outlined in scheme 1.

Hydrolysis and condensation were the key mechanisms of crystal growth in sol-precipitation process. Washing $BaTiO_3$ formed by dilute formic acid helps to eliminate CO_2 absorbed in $BaTiO_3$ during condensation from air.

3.2 *XRD analysis*

Figure 1 shows the XRD pattern of $BaTiO_3$. The crystal structure of $BaTiO_3$ is cubic (JCPDS No. 31-174) because (200) and (002) peaks around $2\theta = 45°$ are not split. The average crystallite size of the nanoparticles was calculated from (110) peak of corresponding XRD peaks by using Scherrer's equation and found to be near 12 nm. The sharp peaks revealed crystalline nature of powder with lattice parameter $a = 4{\cdot}02$ Å and cell volume, $v = 64{\cdot}97$ Å^3. The XRD pattern shows background in the region 20–40°. This may be due to the reason that a thin layer of the nano powder was spread on the glass slide placed in the sample holder for XRD studies, resulting in large scattering of X-rays in this region. For measuring the dielectric constant, sintering was carried out at 400 °C for 12 h and crystallite size was measured by repeating XRD. It was found that there was no remarkable change in average crystallite size.

3.3 *Variation of parameters*

Various process parameters such as concentration of reactants, stirring time and amount of TMAH during the reaction for the formation of $BaTiO_3$ were studied, using

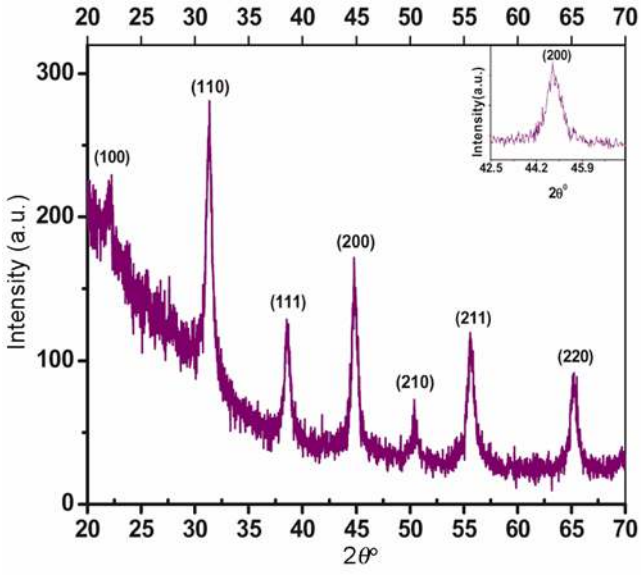

Figure 1. XRD pattern of $BaTiO_3$.

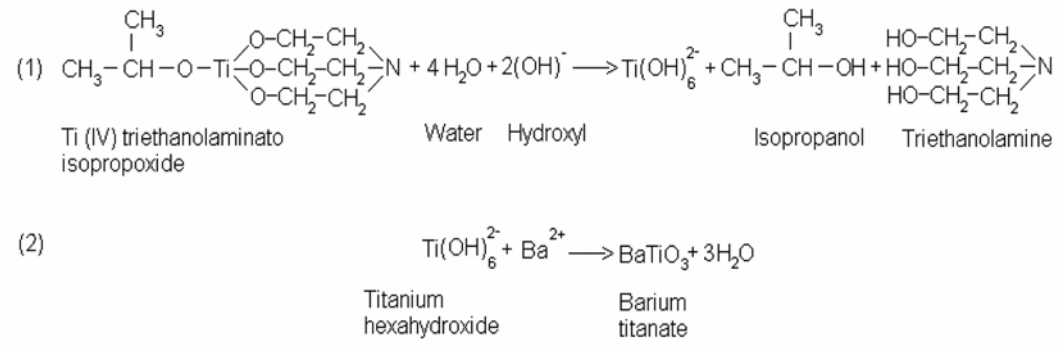

Scheme 1.

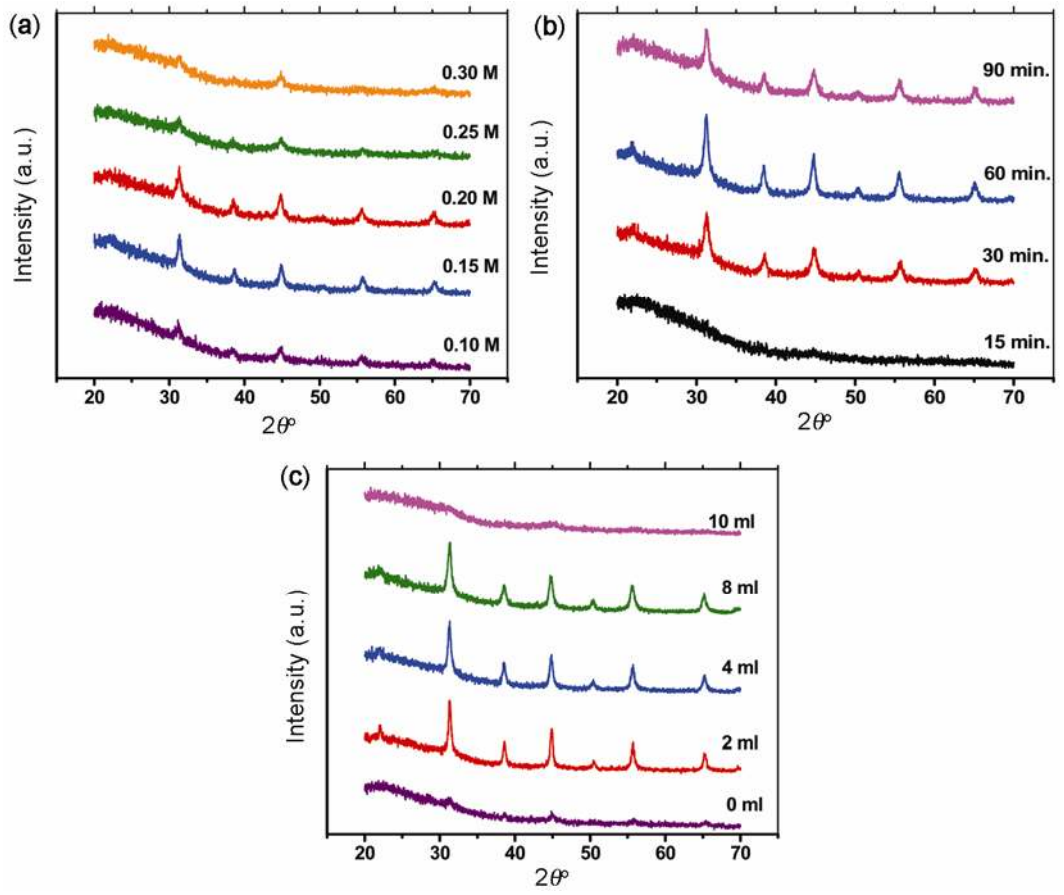

Figure 2. XRD patterns of $BaTiO_3$ nanoparticles synthesized keeping Ba/Ti = 1·02: (**a**) at varying concentrations at fixed stirring time of 1 h and addition of 4 mL TMAH; (**b**) at varying stirring times at 0·2 M fixed concentrations of reactants and 4 mL TMAH and (**c**) at varying mL of TMAH at 0·2 M fixed concentrations of reactants and stirring time 1 h.

XRD techniques by varying one parameter and keeping the other parameters constant.

3.3a *Effect of concentration of reactants*: Concentration of $Ba(OH)_2 \cdot 8H_2O$ and Ti(IV) triethanolaminato isopropoxide were varied from 0·1 to 0·3 M, keeping the molar ratio of Ba : Ti in the mixture always equal to 1·02 and stirring time as one hour and addition of 4 mL TMAH. The XRD pattern of $BaTiO_3$ formed are as shown in figure 2(a). The pattern indicates that crystalline nanoparticles are formed only when molarities of $Ba(OH)_2 \cdot 8H_2O$ and Ti(IV) triethanolaminato isopropoxide are 0·15 and 0·2 M. In the other concentrations studied, there are no sharp and clear peaks. Therefore, 0·2 M $Ba(OH)_2 \cdot$

$8H_2O$ and 0·2 M Ti(IV) triethanolaminato isopropoxide were mixed keeping the ratio of Ba : Ti equal to 1·02 in subsequent preparations for the adequate formation of $BaTiO_3$.

3.3b *Effect of stirring time*: Stirring time was varied from 15 to 90 min by reacting 0·2 M reactants keeping molar ratio Ba : Ti equal to 1·02. The XRD pattern of $BaTiO_3$ formed is shown in figure 2(b). The pattern shows that there is no appreciable change in the formation of crystalline $BaTiO_3$ when stirring time was between 30 and 90 min. There was no formation of BT when the stirring time was 15 min. However, stirring time of 60 min was used in all subsequent preparations of the formation of $BaTiO_3$. Stirring time was not extended above 90 min since the volume of the reaction mixture reduces during stirring due to evaporation.

3.3c *Effect of volume of TMAH*: Volume of TMAH was varied from zero to 10 mL by reacting 0·2 M each of reactants keeping molar ratio of Ba : Ti equal to 1·02 and stirring time as 1 h. XRD pattern of the $BaTiO_3$ formed are shown in figure 2(c). The pattern reveals that crystalline monophasic nanoparticles were obtained when volume of TMAH added was 2 to 8 mL. Zero and 10 mL of TMAH did not allow the formation of $BaTiO_3$. Therefore, 4 mL of TMAH was added in all consequent reactions for the synthesis of $BaTiO_3$.

3.4 *Effect of calcination*

Five samples of $BaTiO_3$ nanoparticles were prepared as per the procedure given in the experimental §2.2 and they were calcined at different temperatures from 100–800 °C for 12 h to evaluate the thermal stability of $BaTiO_3$ nanoparticles. The XRD scan was done at room temperature. The XRD patterns of $BaTiO_3$ formed are as shown in figure 3. The $BaTiO_3$ peaks were not altered till 600 °C temperature, demonstrating the good thermal stability. This shows that $BaTiO_3$ formed by calcination from 100 to 600 °C was crystalline, monophasic and cubic in structure. However, the sample calcined at 800 °C temperature shows the splitting of the peaks showing the change in the structure of the $BaTiO_3$. The investigation of this sample which is calcined at 800 °C is in progress and findings will be published later.

3.5 *Field emission scanning electron microscopy (FE–SEM) and energy dispersive X-ray spectroscopy (EDX) analysis*

The particle size and morphology of $BaTiO_3$ prepared were analysed using SEM. The SEM imaging results in both improved spatial resolution and minimized sample charging and damage due to narrower probing beam. A thick suspension of $BaTiO_3$ nanoparticles were spread on a carbon conductive tape attached to the surface of SEM brass stub. The particles on the stub were coated with gold–palladium by plasma sputtering for 3 min for the preparation for FE–SEM imaging. The FE–SEM image of $BaTiO_3$ nanoparticles prepared is shown in figure 4(a). The particles are spherical in shape and average particle size is 24 nm.

EDX is as shown in figure 4(b). It confirms that the nanoparticles are essentially composed of elements like Ba, Ti and oxygen**.** The peaks of Cu/Zn from the brass grid used, the peak of Au from the coating of powder in the SEM experiment and the peaks of C from the chemisorbed CO_2 impurities were also observed. Omitting these peaks, the chemical composition of $BaTiO_3$ is shown in table 1.

3.6 *Transmission electron microscopy (TEM) and selected area electron diffraction (SAED) analysis*

In order to further investigate the particle morphology and size of particle in BT, TEM image was taken. This is shown in figure 5(a). The TEM specimen was prepared

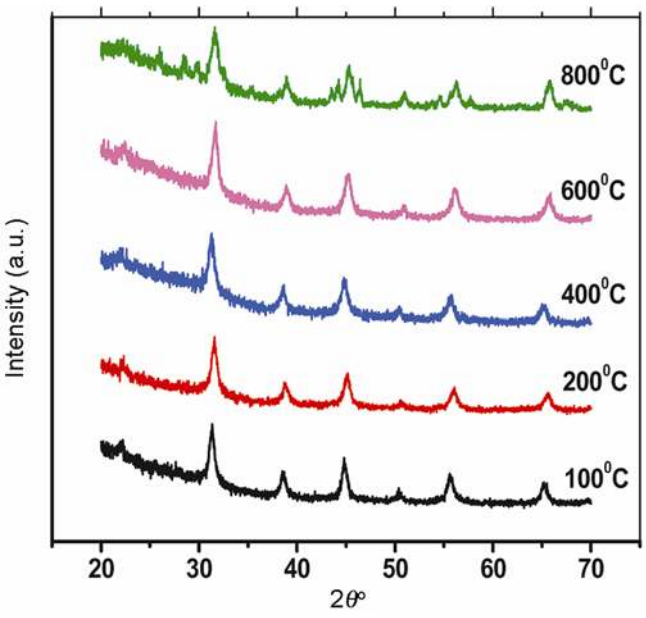

Figure 3. XRD graph of $BaTiO_3$ calcined at different temperatures.

Table 1. Elemental composition table from EDX.

Element	Weight (%)	Atomic (%)
O K	44·19	80·10
Ti K	35·21	07·43
Ba L	20·60	12·47
Total	100·00	100·00

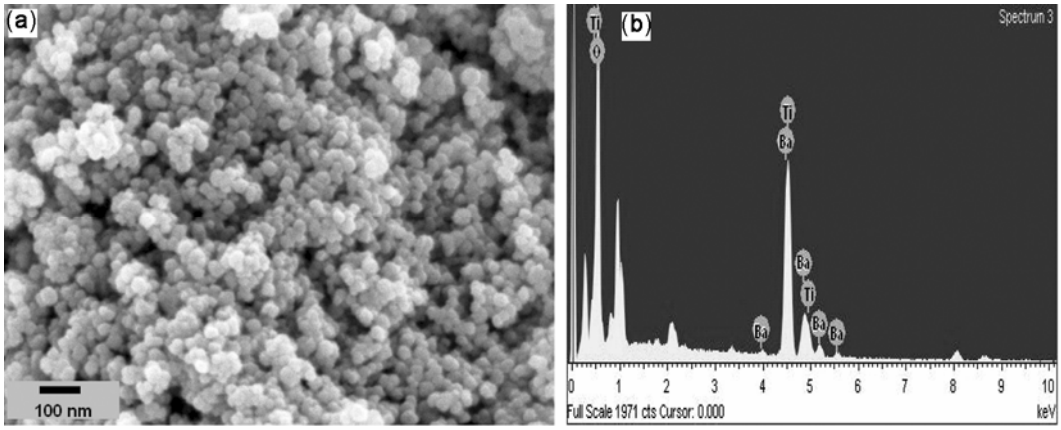

Figure 4. (**a**) FE–SEM image of BT nanoparticles and (**b**) EDX of BT nanoparticles.

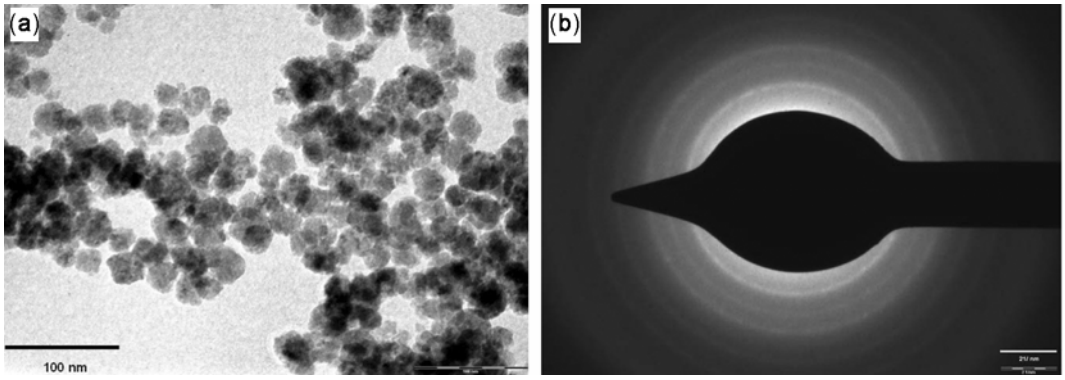

Figure 5. (**a**) TEM imaging of BT nanoparticles and (**b**) SAED of BT nanoparticles.

by dispersing synthesized BT particles in ethanol, then sonicating it in an ultrasonic generator. The particles were picked up using carbon coated copper grid and examined. The TEM instrument was equipped with a system performing SAED to further characterize nanostructure of powder. The TEM image shows that synthesized nanoparticle size is between 23 and 32 nm and spherical in shape besides there exists some agglomerates. As size of the individual nanoparticle is up to 32 nm, it suggests that the synthesized particles were polycrystalline.

Figure 5(b) shows SAED pattern of $BaTiO_3$. The circular bright continuous rings in the SAED pattern corroborate the fact that particles were nanosized and confirm the crystalline nature of nanoparticles. All electron diffraction rings matched with the $BaTiO_3$ cubic phase (Wei *et al* 2008a; Anuradha 2010).

3.7 *Dynamic light scattering (DLS) analysis*

DLS is a technique used for particle size and size distribution studies. We have used this technique for the particle size distribution of $BaTiO_3$ nanoparticles. Figure 6 shows that 65% of the particles were up to 35 nm in size and others were above this size. The maximum size of the nanoparticles are about 100 nm as observed in the figure.

3.8 *FT–IR analysis*

The defective structure and impurity have a significant role in the crystal structure and properties of nanosized $BaTiO_3$ synthesized by chemical route. The $BaTiO_3$ nanoparticles (1 wt%) were mixed thoroughly with IR grade dehydrated KBr in a mortar and pestle. A pellet was prepared using a hydraulic press at 5 ton pressure. The FT–IR spectra of the samples thus prepared is shown in figure 7.

The stretching vibrations were observed at 3396, 1586, 1351 and 583 cm^{-1}. The peaks at 3396 and 1586 cm^{-1} may be attributed to OH group. The peak 1351 cm^{-1} may be assigned to carbonate group whereas peak at 583 cm^{-1} may be attributed to TiO_6 octahedra of $BaTiO_3$ (Arya *et al* 2003; Cernea 2005; Maensiri *et al* 2006; Wei *et al* 2008b).

The OH, CO_2 and CO_3 peaks were reduced in the sample of $BaTiO_3$ when calcined at 600 and 800 °C. The addi-

tional peaks at 861 cm^{-1} in the IR spectrum at 800 °C may be due to metal–oxygen band stretching. These results reveal that $BaTiO_3$ prepared by the present method at 100 °C contains impurities such as adsorbed H_2O, hydroxyl group and carbonate, whereas $BaTiO_3$ calcined at 800 °C is free from these impurities.

3.9 *TG–DTA analysis*

The thermogravimetric (TG) and differential thermal analysis (DTA) curves of $BaTiO_3$ nanoparticles are as shown in figure 8. The TG exhibits 11% total loss due to H_2O, OH^- ions from $BaTiO_3$ crystal lattice and adsorbed CO_3^{2-} ions in the temperature range from 65–1000 °C, as have been reported (Um *et al* 1997; Lee *et al* 2004). The exothermic DTA peak at 360 °C seems to be associated with removal of OH^- ions from lattice of $BaTiO_3$, as reported (Ryu and Yoon 2007).

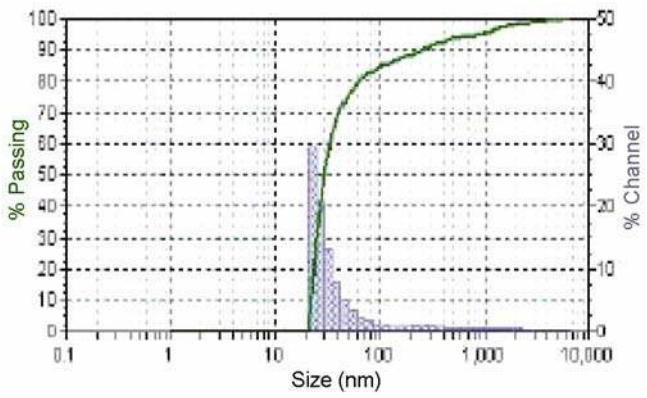

Figure 6. DLS of $BaTiO_3$.

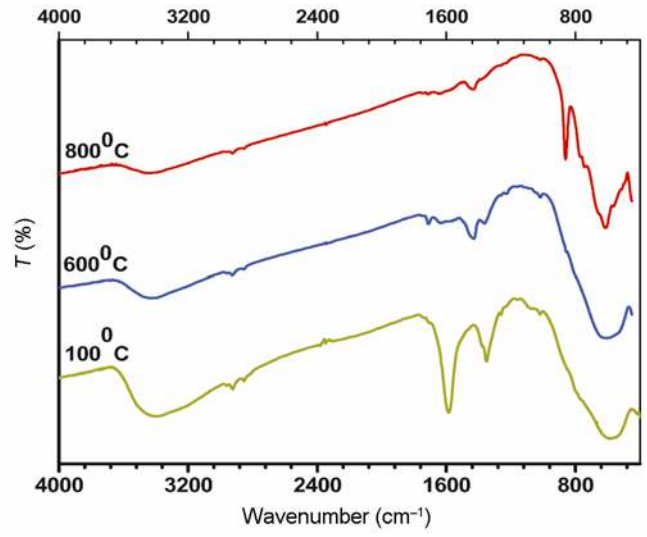

Figure 7. Comparison of FT–IR spectra of BT nanoparticles at different calcination temperatures.

3.10 *Dielectric and electrical behaviour*

The measurement of dielectric constant and dissipation factor were carried out without sintering and were found to be 46·9 and 0·47 at 100 Hz, respectively. At high frequency of 1 MHz, it was observed to be 27 and 0·02, respectively (dielectric spectra of unsintered sample is not reported here). The low value of ε' may be due to voids present in the pellet. To confirm this, pellets were sintered at 400 °C for 12 h and the dielectric measurements were repeated which are discussed below.

3.10a *Dielectric constant*: The ability of the dielectric material to store energy is attributed to the polarization which can result in an increase in capacitance. There are several molecular mechanisms associated with

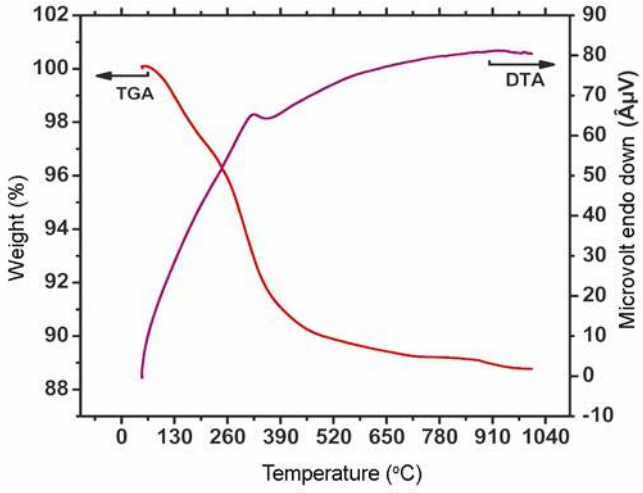

Figure 8. TG–DTA measurements of BT nanoparticles.

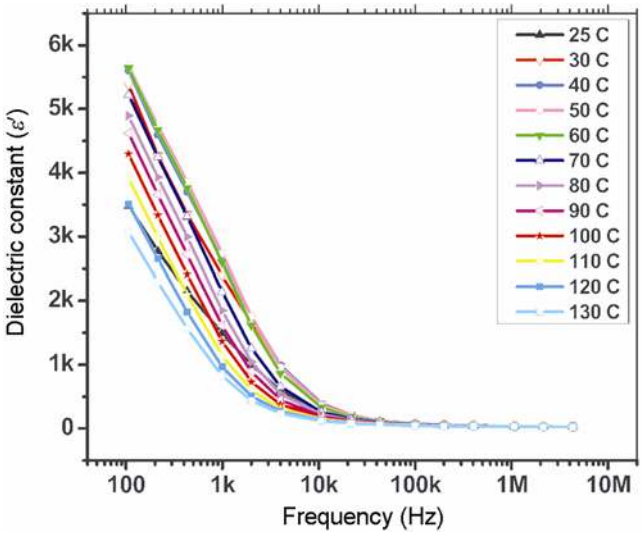

Figure 9. Dielectric constant vs frequency at various temperatures.

polarization, including electronic, ionic, molecular (dipole) and interfacial (space–charge) polarization. It is well known that dielectric properties of every solid are very sensitive to the local electric field distribution in the sample. Therefore, the temperature and frequency dependence of dielectric constant and loss can explore useful information about structure changes, transport mechanism and defect behavior of a solid. Even the slightest chemical and physical change has a dramatic effect on the dielectric properties.

The dielectric studies of $BaTiO_3$ nanoparticles prepared were carried out to see their response to an applied low a.c. voltage in the frequency range of 100 Hz to 4 MHz and with temperature from 25 to 130 °C. The nano powder of $BaTiO_3$ was consolidated into disc (pellet) of 10 mm diameter and 1 mm thickness by applying a uniaxial pressure of 6 tonnes. This pellet was sintered at 400 °C in a muffle furnace for 12 h. The pellet was coated with conducting colloidal silver and dried at 80 °C for two hours. The sample was held between the specially fabricated sample holder having two circular tablet type of gold electroplated copper electrodes which were connected to impedance analyser. The sample holder was kept in a furnace which could be heated to different temperatures and maintained stable within ± 1 °C. The density of the pellet sintered at 400 °C was found to be 2·98 g/cm^3.

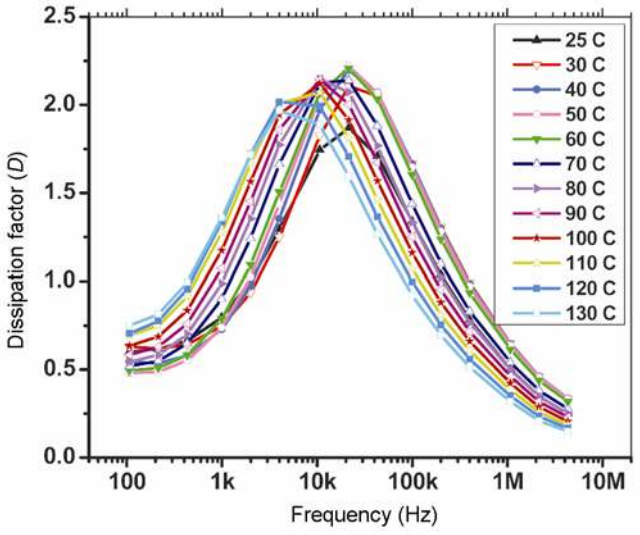

Figure 10. Dissipation factor vs frequency at various temperatures.

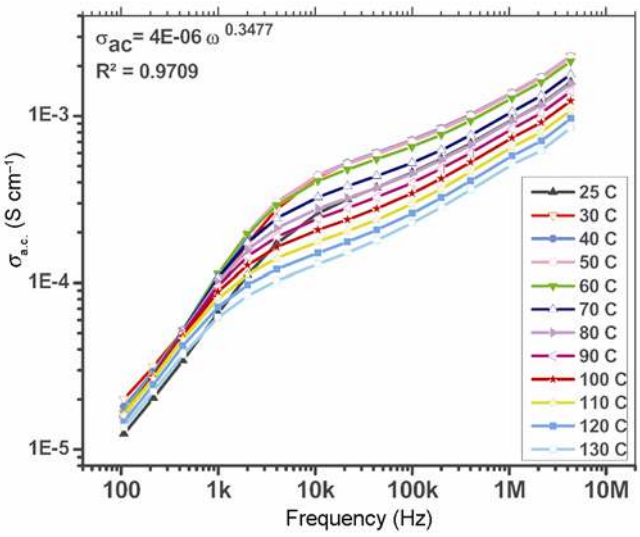

Figure 11. Variation of a.c. conductivity ($\sigma_{a.c.}$) vs frequency at different temperatures.

The variation of dielectric constant against frequency is as shown in figure 9. It is observed that ε' decreases with increase in frequency and increases with increasing temperature up to 50 °C. Thus the curie temperature in this study has shifted to lower temperature 50 °C. A similar observation is reported in case of nanosized $BaTiO_3$ (Kim *et al* 2005). Curie temperature is that at which ferroelectric materials are changed from ferroelectric to non ferroelectric. Generally, for bulk $BaTiO_3$ material, it is 120–130 °C. However, due to size effect, $BaTiO_3$ is stable in cubic phase for nano crystals of $BaTiO_3$. Curie temperature shifts to lower temperature for nanosized $BaTiO_3$ due to various reasons, as reported by Rath *et al* (2008). In the present case curie temperature is found to be 50 °C. The ε' decreases as temperature is further increased. The highest value of ε' at 100 Hz is 5679 at 50 °C. The dielectric constant is always maximum at curie temperature. It decreases rapidly with increase in frequency. The lowest value of ε' is recorded to be 23·8 at 130 °C and 4 MHz.

3.10b *Dissipation factor*: The dissipation factor, *D*, of any material describes quantitative dissipation of the electric energy due to different physical processes such as electrical conduction, dielectric relaxation, dielectric resonance and losses from nonlinear processes such as hysteresis (Burfoot 1967). When we measure the dielectric loss at a single frequency, we cannot, in general, distinguish between them. They all give rise to just one measurable quantity, namely, the total measured *D*.

The variation of *D* against frequency is shown in figure 10. It is observed that *D* increases with increasing temperature up to 50 °C. *D* increases with increasing frequency and attains highest value at around 10 kHz. The relaxation peak is clearly observed at around this frequency for all the temperatures. The relaxation peaks move towards higher frequency with increasing temperature up to 50 °C. With further increase in temperature, peaks are observed to move towards lower frequency. *D* value decreased with increasing frequency beyond relaxation frequency. *D* at higher frequencies shows lower values and there is a small change with elevated

temperature. It was noted to vary between 0·48 and 0·60 at 100 Hz and 0·31 and 0·65 at 1 MHz over a wide range of temperature, which is appreciably good.

3.10c *A.c. conductivity*: A.c. conductivity (σ_{ac}) is obtained from the data of dielectric constant (ε') and loss tangent tan δ (or D) using the relation (Goswamy 1996; Raman and Krishna 2010):

$$\sigma_{a.c.} = \varepsilon' \varepsilon_0 \omega \tan \delta,$$

where $\omega = 2\pi f$ is the angular frequency.

Figure 11 represents variation of a.c. conductivity vs frequency at various temperatures on log–log scale. The a.c. conductivity at 100 Hz is 2×10^{-5} S-cm^{-1} at room temperature (30 °C). It increases with increasing frequency. A dispersive region at high frequencies is observed where the a.c. conductivity can be roughly described by a power law $\sigma(\omega) \propto \omega^n$ with $0 < n < 1$. The nanocrystalline materials are compact polycrystalline materials. In these, the interfaces between like grains and unlike grains exist. This can lead to the formation of ionic space charge layers and thus to an even more enhanced a.c. conductivity.

Figure 12 shows the variation of a.c. conductivity vs temperature. It is observed that the a.c. conductivity increases with increasing temperature till 50 °C and decreases when temperature is increased further. The growth in conductivity is faster till 10 kHz and slow thereafter. This is attributed to free charge carriers and higher density of interface states due to rise in temperature. These states contribute charge carriers due to ionization and could also function as conduction centers for the transport of charge carriers (Berger 2004).

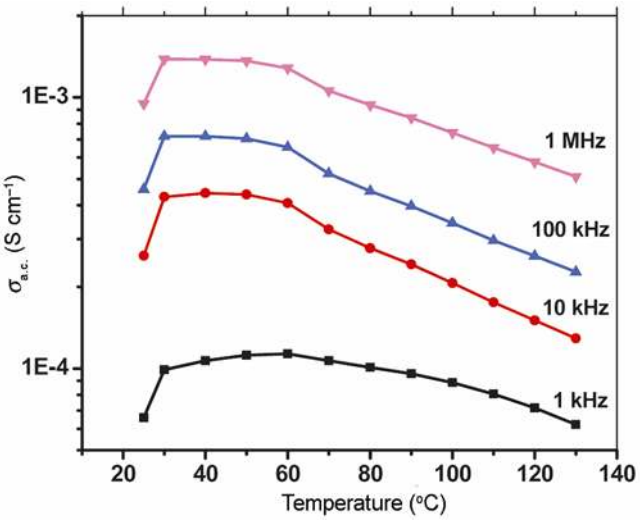

Figure 12. Variation of a.c. conductivity ($\sigma_{a.c.}$) vs temperature at different frequencies.

3.10d *Impedance*: Impedance (Z) is a measure of the overall opposition of a circuit to current. In other words, it indicates how much the circuit impedes the flow of current. It is like resistance but it also takes into account the effects of capacitance. Figure 13 shows the variation of Z against frequency. Z is seen to be $3{\cdot}4 \times 10^5$ ohms at 100 Hz at room temperature (30 °C). Thus a drop is observed in Z, as frequency increases up to 50 °C, as expected according to the reasons explained above. Further, at constant frequency, Z is observed to decrease with increasing temperature as shown in figure 14. The decrease in impedance is pronounced in lower frequency region. This results in larger increase of a.c. conductivity in low frequency range as compared to higher frequency region.

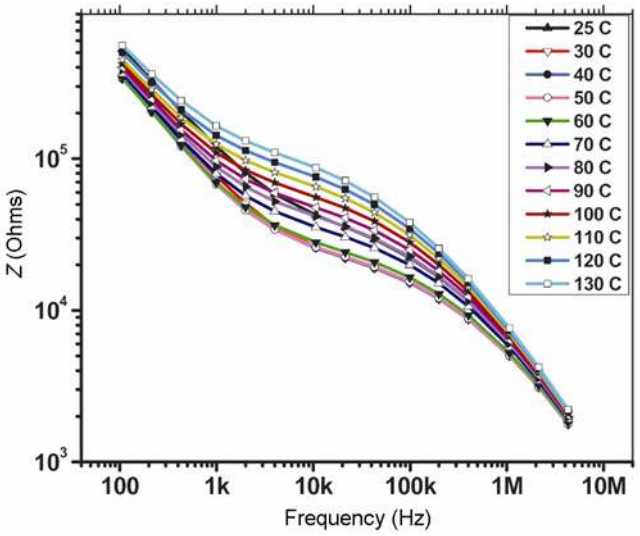

Figure 13. Variation of impedance Z vs frequency at different temperatures.

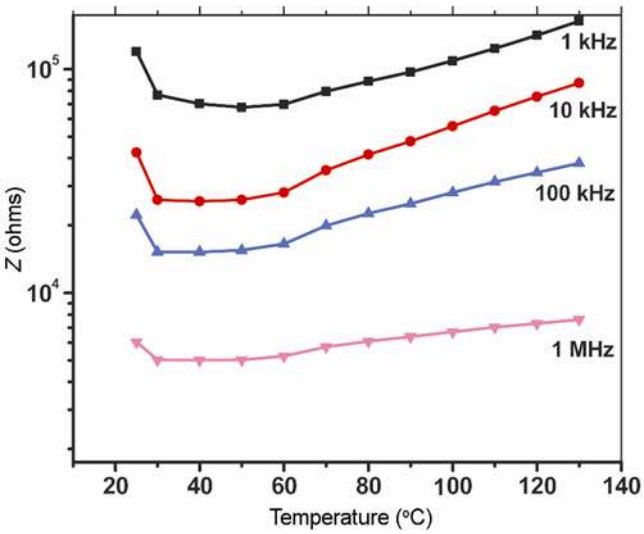

Figure 14. Variation of impedance Z vs temperature at different frequencies.

4. Conclusions

The $BaTiO_3$, prepared by interaction of Ti(IV) triethanolaminato isopropoxide in methanol with hydrated $Ba(OH)_2 \cdot 8H_2O$ in alkaline media containing TMAH using sol-precipitation method, was found to be nanoparticles. The average crystallites were 12 nm as determined by XRD. These particles were found to be spherical and homogeneous with cubic structure. The particle size was 23–31 nm as observed from SEM and TEM. The dielectric constant and dissipation factor of $BaTiO_3$ nanoparticles were found be 5379 and 0·63 at 100 Hz, respectively. Thus, it can be useful dielectric material for industrial application.

Acknowledgements

The authors are thankful to the SAIF Center, Indian Institute of Technology-Mumbai (IIT-B) for allowing them to use the FE-SEM/TEM facilities. Material Science Department, Tata Institute of Fundamental Research (TIFR), Mumbai, for permitting them to use the XRD facilities. They are grateful to the UGC, Govt of India, for granting the FIP fellowship to R H Upadhyay.

References

Anuradha T V 2010 *Coden Ecjhao E-Journal of Chemistry* **7** 894 (http://www.e-journals.net)

Arya P R, Jha P and Ganguli A K 2003 *J. Mater. Chem.* **13** 415

Berger S 2004 *Encyclopaedia of nanoscience and nanotechnology* (ed.) H S Nalwa (New York: American scientific Publishers) Vol. 2, p. 371

Burfoot J C 1967 *Ferroelectrics: an introduction to the physical principles* (London: Van Nostrand Publisher)

Cernea M 2005 *J. Optoelectr. Adv. Mater.* **7** 3015

Feng X, Sayle D C, Wang Z L, Paras M S, Santora B, Sutorik A C, Sayle T X T, Yang Y, Ding Y, Wang X and Her Y -Sh 2006 *Science* **312** 1504

Frey M and Payne D 1996 *Phys. Rev. B, Cond. Matter.* **54** 3158

Goswamy A 1996 *Thin film fundamentals* (New Delhi: New Age International Publishers Ltd)

Guangneng F, Lixia H and Xueguang H 2005 *J. Cryst. Growth* **279** 489

Hanemann T, Gesswein H and Schumacher B 2011 *Microsyst. Technol.* **17** 195

Kim C -S *et al* 2005 *J. Korean Phys. Soc.* **46** 308

Kobayashi Y, Kurosawa A, Nagao D and Konno M 2009 *Polym. Eng. Sci.* **49** 1069

Lee B I, Badheka P, Yoon D H, Magadala V and Wang M 2004 *J. Ceram. Proc. Res.* **5** 127

Maensiri S, Nuansing W, Laokul P, Klinkaewnarong J and Khemprasit J 2006 *J. Colloid & Interface Sci.* **297** 578

Raman S G and Krishna P S 2010 *Synthesis* **2** 72

Rath M K, Pradhan G K, Pandey B, Verma H C, Roul B K and Anand S 2008 *Mater. Lett.* **62** 2136

Ryu S -S and Yoon D -H 2007 *J. Mater. Sci.* **42** 7093

Segal D 1997 *J. Mater. Chem.* **7** 1297

Setter N and Waser R 2000 *Acta Mater.* **48** 151

Shahini S, Askari M and Sadrnezhaad S K 2011 *Bull. Mater. Sci.* **34** 1189

Subbarao E C, Prasad V C S and Veerbhadra Rao K 1981 (eds) J M Honig and C N R Rao (New York: Academic Press) p. 217

Um M -He, Lee C -T and Kumazava H 1997 *J. Ind. & Eng. Chem.* **3** 251

Upadhyay R H and Deshmukh R R 2013 *Adv. Mat. Res.* **2** 49

Wei X, Xu G, Ren Z, Shen G and Han G 2008a *J. Am. Ceram. Soc.* **91** 3774

Wei X, Xu G, Ren Z, Shen G and Han G 2008b *J. Am. Ceram. Soc.* **91** 315

Zhao Z, Buscaglia V, Viviani M, Buscaglia M T, Mitoseriu L, Testino A, Nygren M, Johnsson M and Nanni P 2004 *Phys. Rev.* **B70** 024107-1-8